Interdependence of initial cell density, drug concentration and exposure time revealed by real-time impedance spectroscopic cytotoxicity assay†

C. Caviglia,[a] K. Zór,[a] S. Canepa,[a] M. Carminati,[b] L. B. Larsen,[a] R. Raiteri,[c] T. L. Andresen,[a] A. Heiskanen[a] and J. Emnéus*[a]

Received 16th January 2015,
Accepted 31st March 2015

1. Introduction

Cancer is a pathological condition characterized by uncontrolled division of abnormal cells, invasion into the nearby tissue and ultimately spreading through the lymphatic system or bloodstream.[1] Chemotherapy is based on the administration of drugs that induce cell death in cancer cells. One of the major challenges in the development of anti-cancer therapies is finding the optimum dose of the drug that maximizes cancer cell death with minimum side effects.[2] In pre-clinical studies, several well established cell-based *in vitro* assays are regularly used for the evaluation of the effects of chemotherapeutic drugs on cell proliferation, viability and cytotoxicity.[3–7]

The majority of the standard assays, *e.g.* MTS (3-(4,5-dimethylthiazol-2-yl)-5-(3-carboxymethoxyphenyl)-2-(4-sulfophenyl)-2*H*-tetrazolium),[5] do not provide kinetic information about the biological events occurring in real-time within the same cell population; moreover, they are invasive and labor intensive. When performing *in vitro* cytotoxicity assays, incubation time, drug concentration and initial cell density are important parameters to consider.[8] It has been observed using traditional cytotoxicity assays that the initial cell density influences the cytotoxic effect of certain anti-cancer drugs in various cell lines.[9–12]

However, there is a lack of studies evaluating the combined effect of the initial cell density, drug concentration and exposure time in real-time using a label-free minimally invasive method, which provides information about changes in adhesion and morphological properties of the same cell population during the onset of cytotoxicity. Cell based electrochemical impedance spectroscopy (EIS) pioneered by Giaever and Keese in the 1980s[13] became a well-established label-free, minimally invasive technique for real-time drug screening and toxicity testing of anti-cancer drugs, detecting cell adhesion, morphological changes as well as cell death induced by cytotoxic compounds in the same cell population acting as its own control.[14–20]

[a]*Department of Micro- and Nanotechnology, Technical University of Denmark, Kgs. Lyngby, Denmark. E-mail: jenny.emneus@nanotech.dtu.dk*

[b]*Dipartimento di Elettronica, Informazione e Bioingegneria, Politecnico di Milano, Milan, Italy*

[c]*Department of Informatics, Bioengineering, Robotics, and System Engineering, University of Genova, Genova, Italy*

†Electronic supplementary information (ESI) available. See DOI: 10.1039/c5an00097a

Doxorubicin (DOX), an anthracycline-based antibiotic widely used in the treatment of a broad range of solid tumours as well as acute leukaemia and malignant lymphoma,[21] has been shown to have decreased cytotoxic activity with increased cell density, defined as the 'positive inoculum effect'.[9,11] EIS studies are mainly focused on the dose and/or time dependence of a drug on the specific cell density.[14,17,18] Therefore, the scope of this work was to investigate the time dependent effect of different concentrations of DOX, used as a model anti-cancer drug, on several initial cell densities of HeLa cells using EIS. The obtained EIS data were compared with the traditional end-point cell viability assay (MTS assay), evaluating the toxic effect on mitochondrial functions, and with data from experiments performed in perfusion culture given the increasing popularity of microfluidic lab-on-chip devices.[22–26]

2. Results and discussion

2.1. Optimization of cell density for EIS based cytotoxicity assay

In order to perform successful cytotoxicity determination, the initial cell density needs to be considered[8] since it has been shown to influence the action of certain drugs.[8,9,12,27] Moreover, when developing an EIS-based assay, adhesion properties and the proliferation rate of the used cell line need to be studied in relation to the biological effect of interest (*e.g.* cytotoxicity) in order to define the optimum initial cell density. In EIS-based cytotoxicity assays, the initial cell density has to provide a control growth curve characterized by a stable steady state for the duration of the experiment dependent on the rate of drug-induced cell death. The initial cell density was optimized to provide enough space for the cells to steadily multiply during incubation with the drug. We investigated the correlation between the cell density and the cell index (defined in section 3.6) values by seeding different HeLa cell densities (1000, 12 500, 35 000, 75 000, 100 000 and 160 000 cells cm^{-2}). The different cell densities were continuously monitored for 38 hours, while the control experiment was performed using only cell culture medium.

Fig. 1A shows the cell index increase during 38 h impedance monitoring of adhesion and proliferation of HeLa cells initially seeded at different densities. The first hours provide a good indication of the cell adhesion and spreading that take place immediately after seeding. These processes induce a rapid cell index increase during the first 5 hours as can be seen in Fig. 1A.

In analogy to what has been reported earlier,[14] our results show that cell adhesion and spreading can be considered completed after approximately 5 h, *i.e.* the determined cell index value reflects the total number of seeded and adhered cells.

It can be seen that at high initial cell densities (160 000 cells cm^{-2}), the cell index strongly decreases after having reached its maximum value at about 5 hours from cell seeding. This behaviour suggests that at higher cell densities, yielding a confluent cell layer (complete cell coverage on the

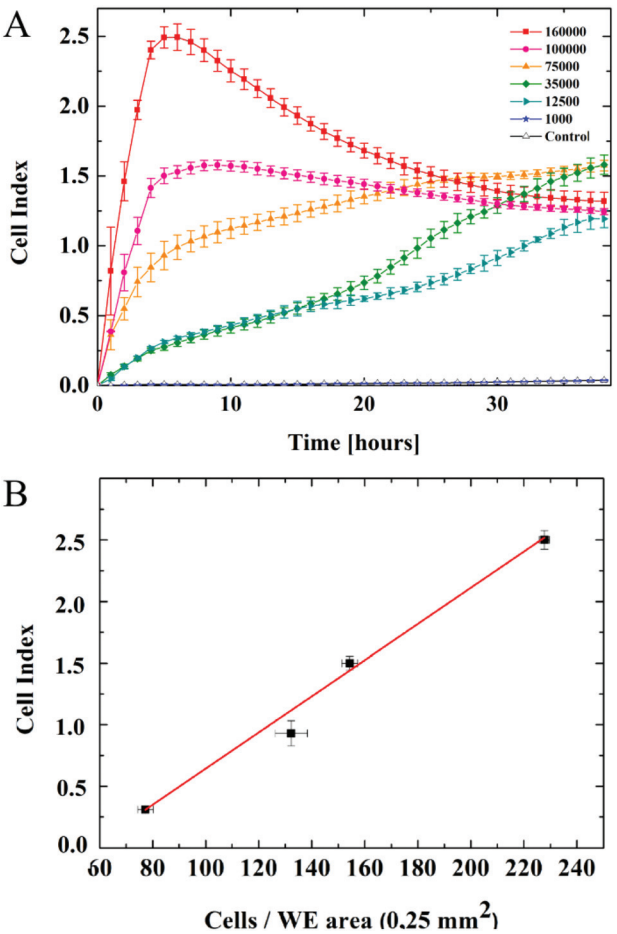

Fig. 1 Optimisation of the initial cell density. (A) Cell index *vs.* time for real-time EIS monitoring of HeLa cell adhesion and proliferation over 38 h. Cells were initially seeded at different densities (1000, 12 500, 35 000, 75 000, 100 000, 160 000 cells cm^{-2}) on laminin coated microelectrode chips. The increase in the cell index during the first hours of the measurement indicates the adhesion and spreading of cells. At high cell densities (160 000 cells cm^{-2}), a strong decrease in the cell index (after 5 h) indicates the upper detection limit of the experimental setup due to the full coverage of the electrode arrays per cell culture well. At low cell density (1000 cells cm^{-2}), the measurements are below the detection limit, the cell index remaining low even after 38 h. Between 12 500 and 100 000 cells cm^{-2} cell density, cell proliferation could be followed up to 38 h. (B) Linear correlation between the cell index and the number of cells on the electrodes was found between 35 000 and 160 000 at 5 h after seeding. Error bars represent s.e.m, $n = 6$.

WEs and/or in the entire culture well), the cell adherence (cell–substrate interaction) is weaker, leading to a lower measured impedance. In other words, under such conditions the upper detection limit of a device is reached, eliminating the possibility to continue monitoring of cell proliferation. We determined the optimal cell density range for this assay to be between 12 500 and 100 000 cells cm^{-2}. Under such conditions, after reaching a steady-state cell index, proliferation could be monitored for a sufficiently long period to facilitate a reliable performance (Fig. 1A). In addition, the number of cells adhering on the IDEs was directly quantified and a linear cor-

relation between the number of cells on the IDE area and the cell index value 5 h after cell seeding was found (Fig. 1B).

2.2. Relationship between initial cell density and rate of cell death

Since traditional endpoint assays have shown that the initial seeding density has an important role when studying the effect of DOX on various cell lines,[9,11,28] we studied the cytotoxicity of DOX concentrations on several HeLa cell densities using real-time EIS. Based on the set of growth curves presented in Fig. 1A, four different densities of HeLa cells (12 500, 35 000, 75 000 and 100 000 cells cm^{-2}) were seeded on the microelectrode chip to evaluate the effect of the initial cell density on the rate of cell death at different drug concentrations. Ten hours after cell seeding, different volumes of the DOX stock solution (prepared in 0.1% NaCl) were added into the culture medium to obtain the final concentrations of 1.25, 2.5 and 5 μM chosen based on MTS assays (ESI, Fig. S1†). Simultaneously, control experiments were performed by exposing the cell populations to culture medium only containing 0.1% NaCl. Fig. 2A shows cytotoxicity profiles at different DOX concentrations presented as cell index at an initial cell density of 75 000 cells cm^{-2}. The observed decrease in the cell index is related to both changes in cellular morphology and adhesion, which at a later stage of the cytotoxic effect result in total detachment of cells (ESI S2†).

Each curve provides real-time kinetic information related to the specific response of the cells to the different concentrations of the drug. While 5 and 100 μM of DOX induce fast cell death, 2.5 μM leads to a response that can be divided into two phases. Initially, a significant increase in the cell index is observed, which after 8 hours is followed by a rapid decrease. This initial increase in impedance also observed by others[18,29] might reflect the intensified metabolic activity, increased adhesion properties and/or changes in cell morphology in response to the stress when trying to overcome the apoptosis induced by the accumulation of the drug. The second phase represents cell death. In contrast, the cell index profile related to 1.25 μM DOX does not significantly deviate from the control experiment, where no relevant variations are recorded. Therefore, further experiments were conducted using 2.5, 5 and 100 μM DOX.

In Fig. 2B, it can be observed that 5 and 100 μM DOX give similar IT_{50} values (defined in section 3.6) for all the cell densities under investigation (from 12 500 up to 100 000 cells cm^{-2}). However, when incubating the cells with 2.5 μM DOX, the IT_{50} value increases with increasing cell density. In the case of DOX, there are a number of proposed mechanisms of action, such as intercalation into DNA during cell division and induction of oxidative stress through free radical formation.[30] For 2.5 μM DOX, the cell death might be predominantly induced by intercalation of the drug into DNA,[30,31] which ultimately results in growth inhibition and apoptosis. On the other hand, the faster and cell density independent cell death induced by 5 and 100 μM DOX may be explained by the fact that at this concentration other mechanisms are involved,

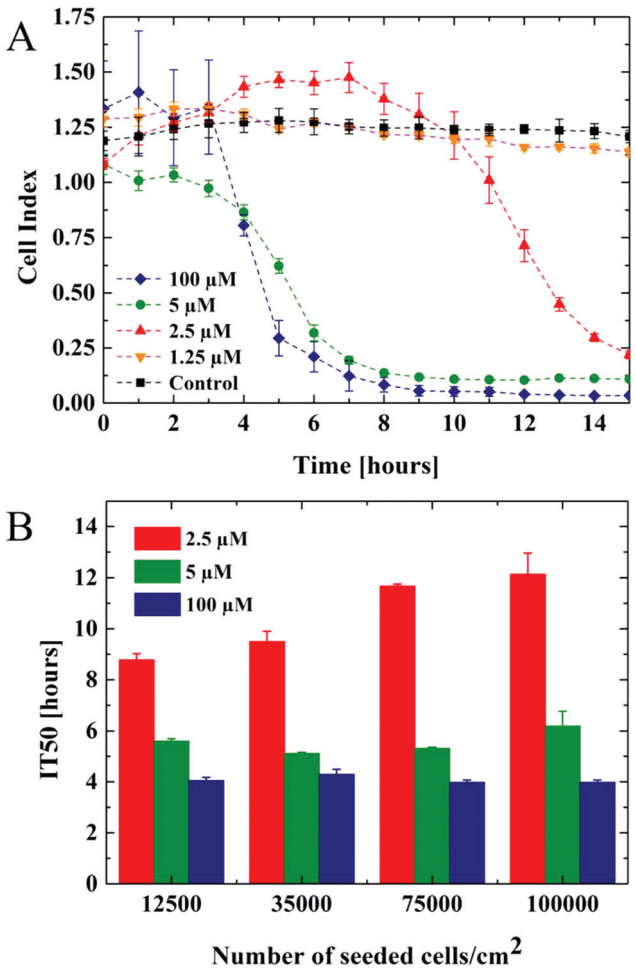

Fig. 2 Effect of the cell density and DOX concentration on cytotoxicity. (A) The cell index decreases after addition of DOX showing the concentration dependent cytotoxic effect of the drug. Cell index profiles of DOX-induced cell death: HeLa cells (75 000 cells cm^{-2}) were seeded on the microelectrode chips and DOX was added 10 hours after cell seeding (t = 0) to achieve a final concentration of 1.25, 2.5 5.0 and 100 μM. (B) IT_{50} values for four different HeLa cell densities (12 500, 35 000, 75 000, 100 000 cells cm^{-2}) exposed to 2.5, 5.0 and 100 μM DOX. The rate of cell death correlated with the cell density at 2.5 μM DOX while this effect cannot be observed at 5 and 100 μM DOX. Error bars represent s.e.m, n = 6.

possibly related to free radical formation.[32] Since one of the proposed mechanisms leading to DOX-induced cell death is dependent on DNA intercalation during cell division,[30] cell proliferation during an assay could play a significant role in the kinetics of cytotoxicity induced by the drug. Considering this, the faster kinetic response at 2.5 μM (about 30% lower IT_{50} value) for the lowest cell density (12 500 cells cm^{-2}) compared with the highest cell density (100 000 cells cm^{-2}) could be related to the fact that at the low cell densities the cells had sufficient space for effective proliferation resulting in faster cell death (Fig. 2B). Another possible explanation of this effect could be the decreased amount of DOX accumulation at higher cell densities.[11]

2.3. Comparison between MTS assay and EIS performed under static and perfusion conditions

Standard spectrophotometric cell viability assays performed in the multiwell format are widely implemented in drug screening and cytotoxicity studies,[33,34] and have thus frequently been used for correlation with real-time impedance data.[35,36] In this work, MTS assays were performed to compare the time-dependent cell death kinetics determined using EIS (ESI, Fig. S3†). MTS time-dependence studies were performed for the four cell densities at different time points (2, 4, 6, 8, 10, 13, 15 and 24 h) after exposure to 5 μM DOX and the results were compared with those obtained by EIS monitoring for the same cell densities (ESI, Fig. S3†). Under the same experimental conditions (cell density, DOX concentration, incubation time) the two methods (EIS and MTS) show similar trends for the different cell densities (ESI, Fig. S3A and B†). However, there is a significant difference between the IT_{50} values determined by the two methods. The IT_{50} values for the MTS assay were over 11 h while those for the EIS monitoring were below 6 h, *i.e.* the response time for the MTS assay is 5 h longer (ESI, Fig. S3C†). Moreover, the kinetic response for 2.5 μM DOX at a cell density of 12 500 cells cm^{-2} was 54% faster for EIS monitoring. The IT_{50} values for higher cell densities (35 000, 75 000, 100 000), obtained using the MTS assay upon exposure to 2.5 μM DOX, could not be compared with EIS data since they indicated 80% cell viability even after 79 h (ESI, Fig. S4†).

Fig. 3 shows a comparison of the calculated IT_{50} values obtained in the MTS assay and EIS monitoring under static conditions as well as comparison to perfusion culture conditions based on our previously published study.[29] The difference in the DOX response time for the two methods is related to the type of biological/chemical/physical event that is being monitored, as previously pointed out in other toxicological evaluations.[35] EIS and MTS assays provide different information about the effect of the drug and measure two different parameters related to cellular functions. While the MTS assay assesses the cell viability based on changes in the mitochondrial activity at later time points, the EIS method responds in real-time to the early changes in the cell–substrate interaction. In the light of the presented results, the two methods provide complementary information for cytotoxicity assessment. On the other hand, the difference in the IT_{50} values between perfusion culture and static conditions, monitoring of cell–substrate interaction, reveals the effect of perfusion conditions in cell based assay.[37,38] The onset of cytotoxicity is significantly delayed under perfusion conditions as indicated by the IT_{50} value close to 30 h. This observation indicates the significance of comparative studies in the light of the increasing popularity of microfluidic cell based assays.

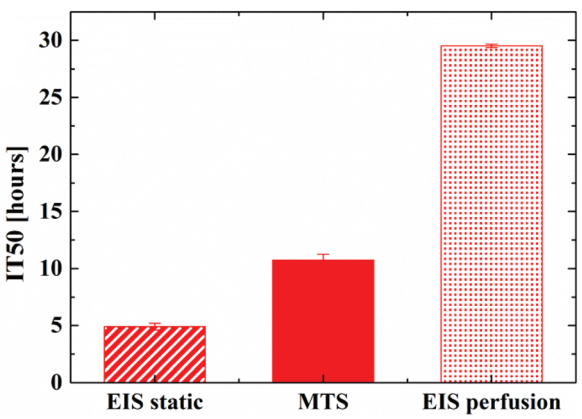

Fig. 3 Cytotoxicity determined with the MTS assay and EIS performed in static and perfusion culture. IT_{50} values were calculated for 75 000 cells cm^{-2} exposed to 5 μM DOX. Error bars represent s.e.m, $n = 6$.

3. Experimental

3.1. Chemicals

Sodium hydroxide, potassium hydroxide, hydrogen peroxide, cell culture tested phosphate buffered saline (PBS), sodium chloride, laminin from the Engelbreth–Holm–Swarm murine sarcoma basement membrane and doxorubicin hydrochloride were purchased from Sigma-Aldrich Corporation (St. Louis, MO, USA). Dulbecco's Modified Eagle Medium (DMEM), trypsin-EDTA (0.05%) and penicillin/streptomycin (P/S) were purchased from Life Technologies Ltd (Paisley, UK). CellTiter 96® Aqueous Non-Radioactive Cell Proliferation Assay (MTS) was purchased from Promega Corporation (Madison, WI, USA).

3.2. Instrumentation, cell culture and experimental setup

The impedance measurement setup is composed of a plastic cell culture unit (Fig. 4A), having a microelectrode chip with an array of 12 interdigitated electrodes (IDE) (Fig. 4B and C), fabricated based on a previously published lithographic process including e-beam evaporation of 150 nm of Au on a 10 nm Ti adhesion layer,[39] a tailor-made 12-channel bipotentiostat with miniaturized PCB and data acquisition software[40] (Fig. 4D; a schematic view of the measurement setup is shown in ESI S5†). Aside from the array of 12 IDEs, each of the independently addressable measurement sites of the microelectrode chip has additional large counter and reference electrodes that have been used in other cell based applications.[41,42]

As schematically presented in Fig. 4A, two 5 mm thick micromilled poly(methyl methacrylate) (PMMA) layers are assembled on top of each other. The lower one is used as a holder for the microelectrode chip, while the upper one, having an opening in the middle, defines a 600 μL well for cell culturing.

A polydimethylsiloxane (PDMS) gasket is placed between the microelectrode chip and the upper PMMA layer to form a liquid tight sealing of the vial. Each of the two combs of the IDEs (shown as working electrodes WEa and WEb in Fig. 4C) is independently addressable and composed of 12 digits (length: 500 μm; width and gap: 10 μm).

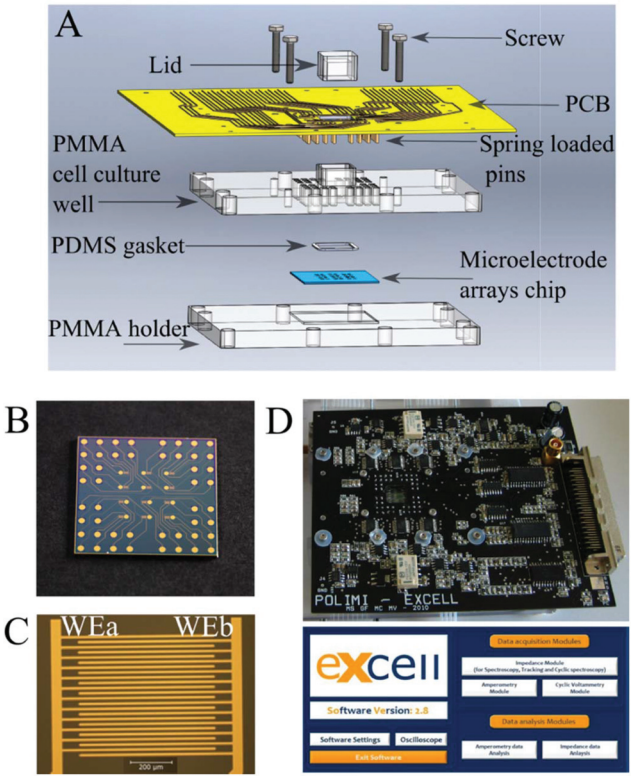

Fig. 4 Impedance measurement setup. (A) Schematic diagram of the cell culture device, with the microelectrode chip integrated between the PMMA holder and the upper layer defining the cell culture well. The PDMS gasket placed between the chip and the upper PMMA layer ensures liquid tight sealing of the well. The custom-made PCB potentiostat is connected to the microelectrode arrays through spring loaded pins. The PMMA lid minimizes medium evaporation and maintains sterile conditions. (B) Photo of the microelectrode chip comprising 12 gold electrode arrays. (C) Microscopic image of one IDE used for coplanar impedance measurements (WEa *vs.* WEb). (D) Photo of the PCB potentiostat and acquisition software.

3.3. Cell culture

HeLa (cat. no. 85060701) cells were purchased from Sigma-Aldrich Corporation (St. Louis, MO, USA). In preparation for experiments, cells were cultured in standard T25 cm^2 flasks with medium exchange regularly every 2 days. Prior to seeding cells on the microelectrode chips, cell suspensions were prepared by standard trypsinization using a trypsin-EDTA solution. Cells were centrifuged for 5 min at 900 rpm and 20 °C followed by resuspension in cell culture medium. The cell number was determined using a standard hemocytometer and the desired cell densities were prepared by diluting the initial cell suspension with fresh culture medium.

Prior to seeding cells in the cell culture device for EIS-based assays, each microelectrode chip was cleaned following the previously described method[43] including a chemical (10 min in a mixture of 25% H_2O_2–50 mM KOH) and electrochemical (potential sweep in 50 mM KOH between −200 mV and −1200 mV) step. Sterilization of the culture well was achieved by a 20 minute treatment with 500 mM NaOH followed by thorough rinsing with PBS. To promote cell adhesion, the chip surface was modified using laminin (20 μg mL^{-1}; 2 h, 37 °C). The applied cleaning procedure facilitated the reusability of the microelectrode chips. Each chip was used for three experiments.

All cell preparations were kept in an ordinary humidified incubator at 37 °C under an atmosphere of 5% CO_2 in air. HeLa cells were cultured in DMEM supplemented with 10% FBS and 1% P/S.

3.4. EIS monitoring protocol

EIS recordings were programmed to be performed continuously at a time interval of 1 hour over the entire experimental period. The applied sinusoidal perturbation potential was set to 200 μV. Full spectra were acquired measuring 30 points in the frequency range of 100 Hz to 100 kHz. 100 kHz was found to be the frequency corresponding to the most sensitive region of the spectra (Fig. 5). At this frequency, the impedance magnitude is influenced by the extracellular resistance and membrane capacitance which are still the primary contribution even when performing measurements up to 1 MHz (ESI Fig. S6†).

To provide a sufficient noise reduction each point was measured with an averaging time of 2 s. The impedance measurements were performed using the coplanar (bipolar) sensing configuration (WEa *vs.* WEb) providing higher sensitivity as previously demonstrated.[44]

3.5. Cytotoxicity assays

For EIS monitoring of the drug-induced cytotoxicity, four different HeLa cell densities (12 500, 35 000, 75 000 and 100 000 cells cm^{-2}) were seeded on the laminin modified microelectrode chips. 10 hours after cell seeding, upon obtain-

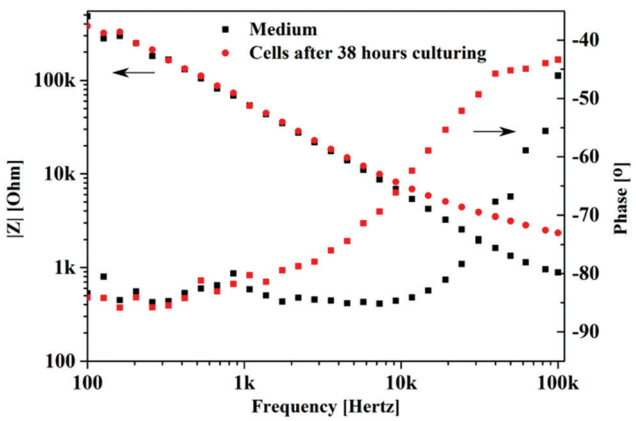

Fig. 5 Impedance spectra recorded for cultured cells (seeded at a density of 75 000 cells cm^{-2}). Bode plots acquired in the frequency range between 100 Hz and 100 kHz (10 data points per decade) using the miniaturized 12-channel bipotentiostat. The cells were cultured for 38 h (cell culture medium as control). To quantify changes in impedance, the cell index is calculated based on complete spectra using eqn (1).

ing an adhering cell layer and a proper baseline for impedance measurements, the anti-cancer drug DOX was added (from a 1 mg mL^{-1} sterile filtered stock solution prepared in 0.1% NaCl) to the cell culture well to obtain the final concentrations of 1.25, 2.5, 5 and 100 μM. These concentrations were chosen based on the dose-dependent values determined using the MTS assay (ESI, Fig. S1†). Control experiments were performed by adding 0.1% NaCl to the cell culture well in the absence of DOX.

Cell viability was measured and quantified by a standard colorimetric MTS assay (performed according to the protocol of the manufacturer) in 96 well plates[5] (covered with aluminium foil to protect from light) using the four different cell densities as during EIS monitoring. 10 hours after seeding, the cells were treated with 5 μM of DOX and incubated. After 2, 4, 6, 8, 10, 13, 15 and 24 h 20 μL of MTS solution were added followed by an additional incubation for 1 h at 37 °C and the absorbance was measured at 490 nm. Control experiments were performed under the same conditions as used during the EIS monitoring. The measured absorbance for each incubated cell population was normalized with respect to the absorbance of the control.

3.6. Data analysis and statistics

Changes in the impedance were expressed using the dimensionless parameter cell index,[17] which represents the maximum value of the normalized impedance based on eqn (1),

$$\text{Cell Index}\,(t) = \max_{i=1,\ldots,N} \frac{|Z(t,f_i)| - |Z(0,f_i)|}{|Z(0,f_i)|} \qquad (1)$$

where $|Z(t, f_i)|$ is the magnitude of the impedance at a given frequency and time point and $|Z(0, f_i)|$ is the magnitude of the impedance at the same frequency at the beginning of the experiment recorded in the absence of cells. In this work, for each time point, the cell index was calculated by analysing the complete spectrum (N = 30). Matlab (R2013a) was used to create specific algorithms for data processing and analysis (for the choice of frequency, see section 3.4).

In order to quantify the time dependence of cell death, we defined the half maximal inhibitory time (IT_{50}) (eqn (2)), analogous to the IC_{50}, as a quantitative measure to indicate how much time is required for the drug to cause 50% decrease in cell viability. The sigmoidal fitting of the data and the IT_{50} values were calculated using the logistic 4-parameter function (Origin (version 9.0)),

$$y = \frac{A_1 - A_2}{1 + \left(\frac{t}{IT_{50}}\right)^p} + A_2 \qquad (2)$$

where A_1 is the initial and A_2 is the final cell index or Abs_{490}, t is the time and p is the slope.

For each experiment, EIS data acquired on the electrodes were processed and averaged. Each experiment was repeated at least two times. Data are presented as average ± standard error of mean (s.e.m).

4. Conclusions

Using EIS-based assays, we clearly demonstrate the interdependence between the initial cell density, the drug concentration and the exposure time as key factors influencing the DOX-induced cytotoxicity. The initial cell density, in combination with the concentration of the anti-cancer drug, determines the time dependent cytotoxicity. At a low (2.5 μM) DOX concentration, a correlation between the initial seeding density and the rate of cell death was found, whereas this was not observed at a higher (5 μM) DOX concentration. Intercalation into DNA during cell division strongly depends on the proliferation rate of the cell population under investigation. Therefore, at low cell densities cells have sufficient space for proliferation, resulting in a faster cytotoxic response compared with higher cell densities. Moreover, our impedance based experimental data were compared with data obtained from MTS assays performed in parallel and we found that the time-dependence of cytotoxicity determined with the two methods differs. EIS measurements detected the cellular response to DOX earlier, which is probably related to the type of event that is being monitored (cell–substrate interaction *versus* mitochondrial activity). This study demonstrates the importance of EIS assays providing additional insight into the cytotoxic activity of drugs unobtainable when only using standard toxicity assays and provided a solid basis for the development of impedimetric cytotoxicity assays in perfusion culture.

Acknowledgements

The used EIS platform is the outcome of EU FP7 project EXCELL (NMP4-SL-2008-214706). We thank Dr Fredrik Melander and Houman Pourhassan for stimulating discussions and suggestions related to cell viability assays and action of DOX, Valeria Tilli and Lucia Montini for their contribution to cell culturing and MTS assays, as well as Francesca Garbarino for performing additional EIS measurements included in the ESI.† We also thank Jesper Scheel for the photographs.

References

1 M. Bacac and I. Stamenkovic, *Annu. Rev. Pathol.: Mech. Dis.*, 2008, **3**, 221–247.
2 R. H. J. Mathijssen, A. Sparreboom and J. Verweij, *Nat. Rev. Clin. Oncol.*, 2014, **11**, 272–281.
3 T. Mosmann, *J. Immunol. Methods*, 1983, **65**, 55–63.
4 E. Borenfreund, H. Babich and N. Martin-Alguacil, *Toxicol. In Vitro*, 1988, **2**, 1–6.
5 G. Malich, B. Markovic and C. Winder, *Toxicology*, 1997, **124**, 179–192.
6 H. Mueller, M. U. Kassack and M. Wiese, *J. Biomol. Screening*, 2004, **9**, 506–515.
7 N. Kramer, A. Walzl, C. Unger, M. Rosner, G. Krupitza, M. Hengstschläger and H. Dolznig, *Mutat. Res.*, 2013, **752**, 10–24.

8 T. L. Riss and R. A. Moravec, *Assay Drug Dev. Technol.*, 2004, **2**, 51–62.
9 T. Ohnuma, H. Arkin and J. F. Holland, *Br. J. Cancer*, 1986, **54**, 415–421.
10 T. Sasaki, Y. Kuroda and F. Hoshino, *J. Radiat. Res.*, 1991, **32**, 202–214.
11 H. Kobayashi, Y. Takemura and T. Ohnuma, *Cancer Chemother. Pharmacol.*, 1992, **31**, 6–10.
12 M. Masquelier and S. Vitols, *Biochem. Pharmacol.*, 2004, **67**, 1639–1646.
13 I. Giaever and C. R. Keese, *Proc. Natl. Acad. Sci. U. S. A.*, 1984, **81**, 3761–3764.
14 L. R. Arias, C. a. Perry and L. Yang, *Biosens. Bioelectron.*, 2010, **25**, 2225–2231.
15 L. Ceriotti, J. Ponti, F. Broggi, A. Kob, S. Drechsler, E. Thedinga, P. Colpo, E. Sabbioni, R. Ehret and F. Rossi, *Sens. Actuators, B*, 2007, **123**, 769–778.
16 Q. Liu, J. Yu, L. Xiao, J. C. O. Tang, Y. Zhang, P. Wang and M. Yang, *Biosens. Bioelectron.*, 2009, **24**, 1305–1310.
17 K. Solly, X. Wang, X. Xu, B. Strulovici and W. Zheng, *Assay Drug Dev. Technol.*, 2004, **2**, 363–372.
18 B. Eker, R. Meissner, A. Bertsch, K. Mehta and P. Renaud, *PLoS One*, 2013, **8**, e57423.
19 J. Hong, K. Kandasamy, M. Marimuthu, C. S. Choi and S. Kim, *Analyst*, 2011, **136**, 237–245.
20 F. Xie, Y. Xu, L. Wang, K. Mitchelson, W. Xing and J. Cheng, *Analyst*, 2012, **137**, 1343–1350.
21 S. K. Carter, *J. Natl. Cancer Inst.*, 1975, **55**, 1265–1274.
22 J.-T. Cao, Y.-D. Zhu, R. K. Rana and J.-J. Zhu, *Biosens. Bioelectron.*, 2014, **51**, 97–102.
23 T. B. Tran, S. Cho and J. Min, *Biosens. Bioelectron.*, 2013, **50**, 453–459.
24 R. Meissner, B. Eker, H. Kasi, A. Bertsch and P. Renaud, *Lab Chip*, 2011, **11**, 2352–2361.
25 S. C. C. Shih, I. Barbulovic-Nad, X. Yang, R. Fobel and A. R. Wheeler, *Biosens. Bioelectron.*, 2013, **42**, 314–320.
26 K. F. Lei, M.-H. Wu, C.-W. Hsu and Y.-D. Chen, *Biosens. Bioelectron.*, 2014, **51**, 16–21.
27 S. Kustermann, F. Boess, a. Buness, M. Schmitz, M. Watzele, T. Weiser, T. Singer, L. Suter and a. Roth, *Toxicol. In Vitro*, 2013, **27**, 1589–1595.
28 Y. Fang, R. Sullivan and C. H. Graham, *Exp. Cell Res.*, 2007, **313**, 867–877.
29 C. Caviglia, K. Zór, L. Montini, V. Tilli, S. Canepa, F. Melander, H. B. Muhammad, M. Carminati, G. Ferrari, R. Raiteri, A. Heiskanen, T. L. Andresen and J. Emnéus, *Anal. Chem.*, 2015, **87**, 2204–2212.
30 D. A. Gewirtz, *Biochem. Pharmacol.*, 1999, **57**, 727–741.
31 S. C. Barranco, *Pharmacol. Ther.*, 1984, **24**, 303–319.
32 F. A. Fornari, J. K. Randolph, J. C. Yalowich, M. K. Ritke and A. Gewirtz, *Mol. Pharmacol.*, 1994, **45**, 649–656.
33 A. L. Niles, R. A. Moravec and T. L. Riss, *Expert Opin. Drug Discovery*, 2008, **3**, 655–669.
34 V. Jurisic and V. Bumbasirevic, *Arch. Oncol.*, 2008, **16**, 49–54.
35 L. Ceriotti, J. Ponti, P. Colpo, E. Sabbioni and F. Rossi, *Biosens. Bioelectron.*, 2007, **22**, 3057–3063.
36 J. Ponti, L. Ceriotti, B. Munaro, M. Farina, P. Colpo, E. Sabbioni, F. Rossi, A. Munari and M. Whelan, *ATLA, Altern. Lab. Anim.*, 2006, **34**, 515–525.
37 G. Cooksey, J. T. Elliott and A. L. Plant, *Anal. Chem.*, 2011, **83**, 3890–3896.
38 E. Jedrych, S. Flis, K. Sofinska, Z. Jastrzebski, M. Chudy, a. Dybko and Z. Brzozka, *Sens. Actuators, B*, 2011, **160**, 1544–1551.
39 M. Dimaki, M. Vergani, A. Heiskanen, D. Kwasny, L. Sasso, M. Carminati, J. a. Gerrard, J. Emneus and W. E. Svendsen, *Sensors*, 2014, **14**, 9505–9521.
40 M. Vergani, M. Carminati, G. Ferrari, E. Landini, C. Caviglia, A. Heiskanen, C. Comminges, K. Zór, D. Sabourin, M. Dufva, M. Dimaki, R. Raiteri, U. Wollenberger, J. Emnéus and M. Sampietro, *IEEE Trans. Biomed. Circuits Syst.*, 2012, **6**, 498–507.
41 K. Zór, A. Heiskanen, C. Caviglia, M. Vergani, E. Landini, F. Shah, M. Carminati, A. Martinez-Serrano, T. Ramos Moreno, M. Kokaia, D. Benayahu, Z. Keresztes, D. Papkovsky, U. Wollenberger, W. E. Svendsen, M. Dimaki, G. Ferrari, R. Raiteri, M. Sampietro, M. Dufva and J. Emnéus, *RSC Adv.*, 2014, **4**, 63761–63771.
42 L. Sasso, A. Heiskanen, F. Diazzi, M. Dimaki, J. Castillo-León, M. Vergani, E. Landini, R. Raiteri, G. Ferrari, M. Carminati, M. Sampietro, W. E. Svendsen and J. Emnéus, *Analyst*, 2013, **138**, 3651–3659.
43 L. M. Fischer, M. Tenje, A. R. Heiskanen, N. Masuda, J. Castillo, A. Bentien, J. Émneus, M. H. Jakobsen and A. Boisen, *Microelectron. Eng.*, 2009, **86**, 1282–1285.
44 C. Caviglia, M. Carminati, a. Heiskanen, M. Vergani, G. Ferrari, M. Sampietro, T. L. Andresen and J. Emnéus, *J. Phys. Conf. Ser.*, 2012, **407**, 012029.